Molecular Crystals and Liquid Crystals
Publication details, including instructions for authors and subscription information:
http://www.informaworld.com/smpp/title~content=t713644168

Optical Properties of Fluorinated Bent-Core Liquid Crystals Confined in Anodic Alumina Nanotubes

Omar G. Morales-Saavedra[a]; María Esther Mata-Zamora[a]; Fernando G. Ontiveros-Barrera[a]; José G. Bañuelos[a]; Roberto Ortega-Martínez[a]; Gerhard Pelzl[b]
[a] Centro de Ciencias Aplicadas y Desarrollo Tecnológico, Universidad Nacional Autónoma de México, CCADET-UNAM, Ciudad Universitaria, México, D. F., México [b] Institut fur Physikalisches-Chemie, Martin Luther University, Halle-Wittenberg, Mühlpforte Halle, Germany

First published on: 19 August 2010

To cite this Article Morales-Saavedra, Omar G. , Mata-Zamora, María Esther , Ontiveros-Barrera, Fernando G. , Bañuelos, José G. , Ortega-Martínez, Roberto and Pelzl, Gerhard(2010) 'Optical Properties of Fluorinated Bent-Core Liquid Crystals Confined in Anodic Alumina Nanotubes', Molecular Crystals and Liquid Crystals, 526: 1, 139 — 155
To link to this Article: DOI: 10.1080/15421406.2010.485533
URL: http://dx.doi.org/10.1080/15421406.2010.485533

Mol. Cryst. Liq. Cryst., Vol. 526: pp. 139–155, 2010

ISSN: 1542-1406 print/1563-5287 online
DOI: 10.1080/15421406.2010.485533

Taylor & Francis
Taylor & Francis Group

Optical Properties of Fluorinated Bent-Core Liquid Crystals Confined in Anodic Alumina Nanotubes

OMAR G. MORALES-SAAVEDRA,[1] MARÍA ESTHER MATA-ZAMORA,[1] FERNANDO G. ONTIVEROS-BARRERA,[1] JOSÉ G. BAÑUELOS,[1] ROBERTO ORTEGA-MARTÍNEZ,[1] AND GERHARD PELZL[2]

[1]Centro de Ciencias Aplicadas y Desarrollo Tecnológico, Universidad Nacional Autónoma de México, CCADET-UNAM, Ciudad Universitaria, México, D. F., México
[2]Institut fur Physikalisches-Chemie, Martin Luther University, Halle-Wittenberg, Mühlpforte Halle, Germany

In the present work, oxalic amorphous porous anodic alumina membranes with highly ordered porous arrays and average nanometric porous dimensions of 70 nm in diameter and 17 microns in depth (nanotubes) were prepared and successfully used as host matrix for fluorinated bent-core liquid crystals. Atomic force microscopy studies were performed on the organic-inorganic hybrid samples in order to explore surface morphology and optimal insertion of these liquid crystalline (LC)-compounds into this environment. The quadratic nonlinear optical (NLO) and spectroscopic properties of the implemented mesogen with the nanotube-like confinement were systematically studied in order to evaluate its optical performance. Bent core molecules have shown interesting optical properties which have not yet been intensively investigated in solid-state hybrid structures. Hence, the obtained hybrid composites represent a promising field of investigation in the route to functional bent-core based materials, where different bent-core mesomorphic structures can be obtained and are of interest for new and improved applications in nanotechnology.

Keywords Bent-core molecules; hybrid materials; liquid crystals; nanostructures; optical properties; porous anodic alumina

Address correspondence to Omar G. Morales-Saavedra, Centro de Ciencias Aplicadas y Desarrollo Tecnológico, Universidad Nacional Autónoma de México, CCADET-UNAM, Apartado Postal 70-186, México, D. F., CP. 04510, México. Tel.: +52-5622-8602, EXT: 1124; Fax: (5255) 56 22 86 37; E-mail: omar.morales@ccadet.unam.mx

1. Introduction

Optics and particularly non-linear optics have emerged as very important research fields providing several high-tech applications in opto-electronics, photonic technologies, and optical data storage and processing [1–5]. During the past two decades, considerable progress has been made in understanding the factors that affect the molecular and material properties for linear and non-linear optical applications; recent investigations have demonstrated that organic materials represent a better alternative due to their fast response times, lower dielectric constants, better processability characteristics, lower production costs and enhanced NLO responses [3–6]. Under this framework, materials such as push-pull polymers, guest-host polymeric structures, organometallic complexes, ferroelectric and anti-ferroelectric LC materials such as bent-core (''banana'') liquid crystals and recently diverse functional organic-inorganic hybrid structures have also been investigated regarding their optical and NLO properties [7–8].

On the other hand, porous anodic alumina (PAA) has been known since the beginning of the twentieth century for its high-tech importance in the industrial anodization of aluminum [9]. More recently, due to its ideal nanopore geometrical arrangements, it was proposed as a promising template for the growth of 1D ordered arrays such as bundles of nanotubes or nanowires [10–12], which constitutes a critical step in the development of operative nanometric devices and prototypes. In fact, PAA templates with porous densities ranging from 10^9–10^{15} pores cm^{-2}, diameters (D) varying from 4 to 250 nm, typical tube lengths (L) ranging between 0.1 to 300 μm, and pore aspect ratios (L/D) from 10 to 1000 [13–16] are routinely prepared following well established fabrication techniques. In recent years a significant number of scientific papers have been published reporting the growth of carbon nanotubes [17–19], metallic nanowires, oxide and chalcogenide semiconductor nanowires [20–24], inside the porous/nanotubes PAA templates. In most of these works the PAA films are basically considered as mechanically inert supports, ready to be filled using a wide variety of techniques, such as the pyrolysis of hydrocarbon compounds, AC-electrochemical deposition or immersion in colloidal suspensions. These approaches work reasonably well in many cases, not taking into account however, the specific chemical composition and properties of the nanopore walls which can play an important role in the definition of alternative synthetic routes for the preparation of a variety of new 1D nanostructures. Several works have been published concerning the physical and chemical characterization, the composition and structure of anodic alumina [25–29]. Although most of that information is spread in different scientific reports, a considerably better understanding of the fundamental properties of these structures has already been achieved, giving rise to new and potential perspectives in emergent applied sciences such as opto-electronics and photonics, which are currently being considered as essential research fields for the development of advanced technological applications. Under this context, we present in this work a comprehensive optical and morphological study of PAA based nanotubes prepared by the oxalic acid route [13–14], which have been filled with optically active fluorine substituted bent-core liquid crystalline compounds. These compounds have been specifically designed for nonlinear optical applications, such as optical second and third harmonic Generation (SHG, THG). The optimal inclusion of these molecular systems into an amorphous inorganic PAA nanotube matrix may provide alternative low cost solid/LC-state optical

hybrid materials for photonic applications and represent a challenging task of current interest.

The experimental results shown in this work have been carried out as a first step in the development of functional organic-inorganic photonic prototypes, and as a practical alternative to expensive inorganic crystals, where the use of specially designed bent-core NLO-LC-molecules plays an important role. The present paper provides experimental evidence concerning the possibility to create organic-inorganic 1D-NLO active hybrid structures implementing PAA templates and functionalized bent-core mesogens in solid state.

2. Experimental Section

2.1. *Characteristics of the Fluorine Substituted Bent-Core LC-Molecule*

Although the synthesis of the first "strongly" bent-core compound can be traced back to 1929 [30,31], their smectic properties were appreciated only after their synthesis by *Matsunaga et al.* in 1993 [32,33]. Soon after, it was realized that due to closed packing requirement bent-core molecules can be polar [34,35]. This polar packing together with director tilt can give rise to chiral layer structures without chirality in the molecular level [36]. In the first few years of experimental studies different 'banana liquid crystal' textures have been observed and labeled as $B_1, \ldots, B_8$, etc. according the chronological order of their observations [37,38]. Several of these phases present antiferroelectric (*AFE*) ground states, either in synclinic-*racemic* or anticlinic-*chiral domain* structures. The *AFE* arrangement can be easily switched by suitable external electric fields, to a ferroelectric (*FE*) state. On a molecular level, the structure of bent-shaped compounds show a non-centrosymmetric distribution of the conjugated π-electrons-system resulting in a permanent dipole moment along the bent direction, which is a key point for NLO-applications [38–43].

In this work, the implemented banana-mesogen corresponds to compound Nr. 9 [44], and was provided by the Halle-group (Germany) [44,45]. The chemical formula of this compound is 1,1,3-phenylene bis[4-(4-noniloxy-3-fluoro-phenylimino-methyl)benzoate] and is schematically represented in Figure 1. This compound was named here **PFB**, due to its polar nature (Polar-Fluorinated-Banana) and to the constituting Phenyl, Fluorine and Benzoate units.

The studied compound exhibits a thermotropic behavior where monotropic phases take place for this particular mesogen, including crystalline (*Cr*-), B_4-, *Sm-CP* and *Sm-X* phases [44]; the thermal properties of this compound are given in Table 1. Furthermore, the presence of two equal electro-donor and electro-acceptor systems linked together such as bis-dipolar molecules makes this compound an interesting candidate for NLO-applications due to its two-dimensional charge-transfer nature.

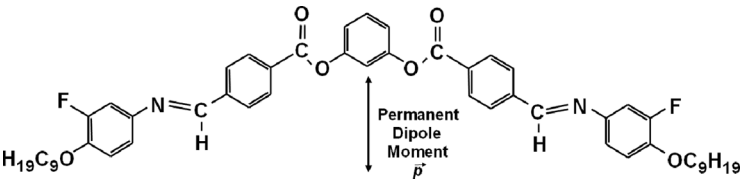

Figure 1. Chemical structure of the symmetrically fluorinated bent-shaped compound (**PFB**).

Table 1. Phase transition temperatures of the **PFB** bent core compound (Nr. 9, from Ref. [44])

Compound	Phase transition temperatures (°C)							
PFB	*Cr*		B_4		*Sm-CP*		*Sm-X*	*I*
	•	123	(•	101)	•	153	•	163

In fact, on a molecular level the structure of these banana-shaped compounds shows a clear non-centrosymmetric density distribution of the conjugated π-electron-system, forming dipoles along the two molecular wings, resulting in a permanent molecular dipole moment $\boldsymbol{p}$ along the twofold symmetry axis. These properties give rise to a polar order in such compounds, which is in principle, equivalent to a non-centrosymmetric arrangement: a fully necessary condition for the occurrence of, for example, quadratic NLO-effects. Specifically, these properties are due to the presence of the Fluorine atom and the carboxyl- and oxy-groups on the molecular wings producing a net polarization along the symmetry axis of the molecular bend direction. Recent studies have proven that such systems lead to the observation of important optical nonlinearities since the nonvanishing components along the conjugation length of the two benzylideneaniline wings produce large molecular hyperpolarizabilities [46–48].

2.2. *Porous Anodic Alumina Template Preparation and Insertion of Bent-Core LC*

High purity aluminum (99.999%, Sigma-Aldrich) foils with a thickness of 0.13 mm were used as starting material. Prior to anodization, the aluminum was annealed under air at 480°C for 1 h. The annealed plates of 10×25 mm were electrochemically polished (1:5 v/v of $EtOH/HClO_4$), and then mounted as the anode in an electrochemical cell using a graphite cathode. The preparation of oxalic porous anodic alumina was carried out using standard conditions widely reported in the literature [13,14,28,29], where 0.3 M of oxalic acid at 40 V was used to induce anodization of Al. The temperature bath was kept at 1°C and the anodization time was fixed to 6 h in order to obtain film thickness of about 17 μm. The aluminum was then electrochemically removed (electrochemical etching in 20 wt% HCl solution, with an operating voltage in the range of 1–5 V) in a circular defined area using elastic O-rings, leaving freestanding alumina windows in mechanically stabilizing Al frames [49]. Thus, porous anodic alumina templates conformed by hexagonal pore arrays with ~138 nm interpore distances formed by self-organization in the anodic alumina are obtained [13]. The circular working surface size was on the order of ~8 mm in diameter. Afterwards, an etching chemical attack via phosphoric acid (0.5 M at 35°C for 35 min) was carried out in order to fully open the nanopores of the anodic alumina, producing the 1D-nanotube like array [50]. This etching process also leads to some pore widening, so the observed pore diameters do not reflect the intrinsic properties of the anodization process. By this methodology, 1D nanotubes varying in the range of 60 to 80 nm in diameter were obtained for the opened barrier layer and the porous cap, respectively. Both surfaces were carefully monitored by AFM in order to assure optimal widening.

Once the 1D nanotube arrays within the anodic alumina-membranes (AAM) were optimally produced, 1.5 mg of the fluorinated bent-core LC were fully dissolved

in 1 ml of toluene in order to obtain a saturated viscous dissolution. The AAM-membranes were mounted with the porous cap placed upwards onto the input tap of a low power vacuum system (KH-07164–30/$\frac{1}{2}$ hp, 5×10^{-2} torr). In order to avoid any damage to the fragile AAM due to excessive low pressure, the membranes were supported by a thin and rigid metallic grid. Afterwards, by using a micropipette, the rounded AAM were fully covered with the bent-core LC-dissolution; the vacuum system was then started and the inclusion of the **PFB**-NLO-molecules within the 1D-AAM nanotubes was mechanically induced. This procedure was repeatedly carried out and a final dissolution drop was placed onto the AAM with the vacuum system turned off, taking advantage of the fact that the AAM-nanotubes had already been damped, favouring the impregnation process and molecular insertion. Subsequently, both the porous and opened barrier layers of the AAM-anodic alumina membranes were carefully cleaned with a toluene-damped optical tissue in order to remove any dissolution overload. The hybrid samples were isolated while drying with a plastic cover in order to avoid atmosphere and temperature variations, and conserved for one to two days at room conditions in closed recipients in a clean-dry-dark environment. Pure AAM were also prepared for reference and calibration purposes.

2.3. *Physical Characterization Techniques*

Standard physical characterization techniques were applied to pure reference AAM and to the AAM/PFB based hybrid samples in order to determine their structural and physical properties according to the following methodology and equipment:

(i) ***AFM-Measurements***: The surface morphology of the films was studied by Atomic Force Microscopy (AFM) (Park AutoProbe CP equipment), where the acquisition of images was performed in contact mode with an interaction force applied between the sample and the AFM-tip of 1.5 nN. The AFM system was equipped with a SiN sharpened Microlever^{TM} tip with typical force constant of $0.05\,N\,m^{-1}$ and resonant frequency of 22 KHz which specify the mechanical characteristics of the used cantilever (typical constants of the instrument). Both the porous cap and barrier layer were carefully monitored by AFM in order to assure optimal quality of the AAM and the insertion of guest molecules.

(ii) ***UV-VIS Spectroscopy Measurements***: Fluorinated bent-core LC were dissolved in spectral quality toluene solvent purchased from Aldrich. UV-Vis absorption spectra of these compounds in solution (using 1 cm quartz cells) and in the AAM solid-state environment were recorded within the 200–1100 nm spectral range on a double beam Shimadzu-260 UV-Vis spectrophotometer, taking air in the reference beam.

(iii) ***Photoluminescent Spectroscopic Measurements***: Similarly, photoluminescent (PL)-spectra were obtained in the 300–900 nm spectral range with a FluoroMax-3, Jobin-Yvon-Horiba fluorimeter. The excitation wavelengths were selected according to the UV-VIS absorption spectra of the liquid or solid state hybrid samples to a convenient wavelength (near the absorption wavelength maximum). Such UV-Vis and PL-studies were initially carried out in order to verify the inclusion of the guest compounds within the AAM porous network and the optical quality of the samples.

(iv) ***Raman Measurements***: An Almega XR Dispersive Raman spectrometer equipped with an Olympus microscope (BX51) was used to obtain the Raman spectra of the samples. An Olympus 50 X objective (N.A. = 0.45) was used as focusing optical system for the Raman laser source; the spot size of the focused laser beam on the sample was $\sim 1.5\,\mu m^2$. The same objective was also implemented as collecting optical system for the back-scattered light in a 180° backscattering configuration. The scattered light was detected by a charge coupled device (CCD) detector, thermoelectrically cooled to − 50°C. The spectrometer used a convenient optical grating (675 lines mm^{-1}) to resolve the scattered radiation and a notch filter to block the Rayleigh light. The pinhole of the monochromator was set at 25 μm and the Raman spectra were integrated over 20 s with a resolution of $\sim 4\,cm^{-1}$. The excitation source was obtained from a Nd:YVO_4 laser (frequency-doubled at 532 nm) and the incident power at the sample was of ∼8 mW.

(v) ***NLO-Measurements***: Finally, selected samples were also studied as active media for quadratic NLO-effects such as SHG. The SHG experimental device is schematically shown in Figure 2, where a commercial high power Q-switched Nd:YAG laser system operating at $\lambda_\omega = 1064\,nm$ with a repetition rate of 10 Hz and a pulse width of $\tau \approx 12\,ns$ (Continuum-Surelite II) was implemented to provide the fundamental wave. Typical pulse powers of 80 μJ were implemented in order to irradiate the film samples, with a variable intensity on the sample that ranged from 60 to $80 MW/cm^2$ and controlled by neutral density filters in order to avoid laser induced damage caused by high intensities of strong focused beams. It was possible to select the desired polarization of the fundamental beam by means of an IR-coated Glan-Taylor polarizer and a quartz-retarder ($\lambda/2$-plate, zero-order). A second polarizer was used as an analyzer, allowing the characterization of the SHG-light. The SHG-wave ($\lambda_{2\omega} = 532\,nm$) was detected by a sensitive photomultiplier tube (PMT-Hamamatsu, R-928) placed behind optical interference filters centered at $532 \pm 5\,nm$. The SHG-device was calibrated by means of a Y-cut α-quartz crystal, wedged along the d_{11}-direction (where $d_{11} = 0.64\,pm\,V^{-1} = 0.5\,\chi^{(2)}_{11}$), which is commonly used as a NLO-reference standard via the Maker-Fringes method [3–4]. All the NLO-measurements were performed at room conditions.

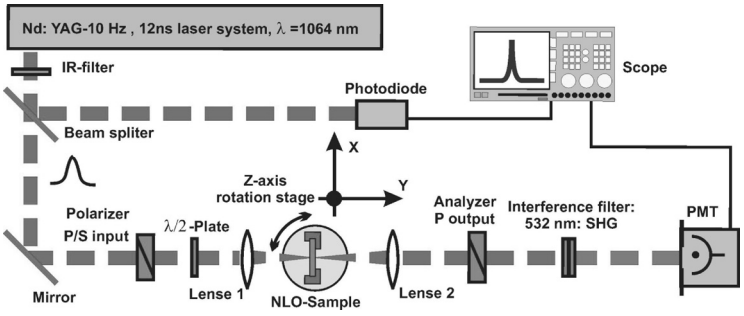

Figure 2. Experimental device used for NLO-SHG measurements in bent-core based AAM hybrid materials.

3. Results and Discussions

3.1. *Morphological AFM–Studies*

A set of pictures of the studied samples are shown in Figure 3, where the **PFB** yellow colored hybrid sample contrast with the pure AAMs transparency.

The morphological AFM-structure of developed reference AAM is shown in Figure 4. The AFM micrographs ($1 \times 1\,\mu m$ resolution) demonstrate in fact that the undoped nanotube arrays obtained for the oxalic anodic alumina template, exhibit average diameters varying from 60 to 80 nm for the opened barrier layer and the porous cap, respectively. Figures 4(a) and 4(b) correspond to a typical porous cap and opened barrier layer, respectively. In both cases well defined geometrical patterns can be observed, where hexagonal structures forming ordered 2D-arrays can be recognized. The opened barrier layer illustrates slightly smaller porous dimensions; this is understandable because after the anodization process, the applied chemical attack selectively operates at different depths within the forming 1D-nanopore walls. In fact porous anodic films contain significant amounts of acid anions incorporated from the anodizing electrolyte and the distribution of electrolyte anions across the cell material is not uniform. A region of Al oxide extending from the pore wall contains relatively large acid anion content. At the same time an inner region of oxide is relatively pure Al oxide [25–29]. All this means that the upper walls of the nanopores present drastic physical and chemical structural changes, compared to that suffered by the lower ones, which allow a faster degradation produced by the phosphoric acid.

Once the higher quality AAMs have been selected; the insertion of the bent-core LC was properly carried out. Figure 4(c) shows an AFM micrograph example of the fluorinated bent-core based AAM-hybrid nanocomposite. It is overall observed at the selected resolution level, that the **PFB**-moleculess were successfully and homogeneously embedded within the AAM-nanotube array by means of the implemented mechanical method, as the nanopore array appear completely filled and conserving the nanopore geometrical shape. The observed extreme inclusion of the **PFB**-NLO-compounds occurs in principle due to the fast vaporization of the solvent used and to the intrinsic viscosity of the dopant dissolution, releasing an adequate inclusion of the **PFB**-compounds within the AAM-nanotubes. According to several experiments, it is concluded that optimal Toluene/**PFB** dissolution ratios should be achieved in order to regulate the viscosity and concentration of the dopant dissolutions, obtaining consequently best possible conditions for the insertion of the

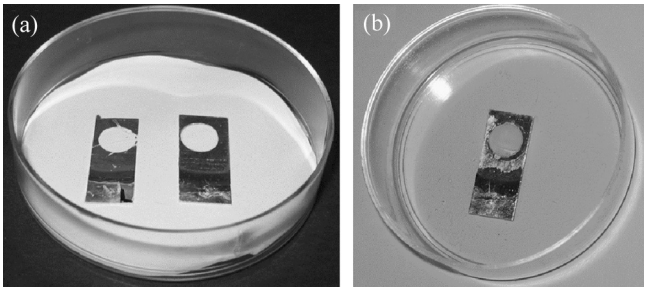

Figure 3. Set of pictures of: (a) pure AAMs used for reference and calibration purposes (transparent), and (b) a PFB bent-core filled AAM sample (opague).

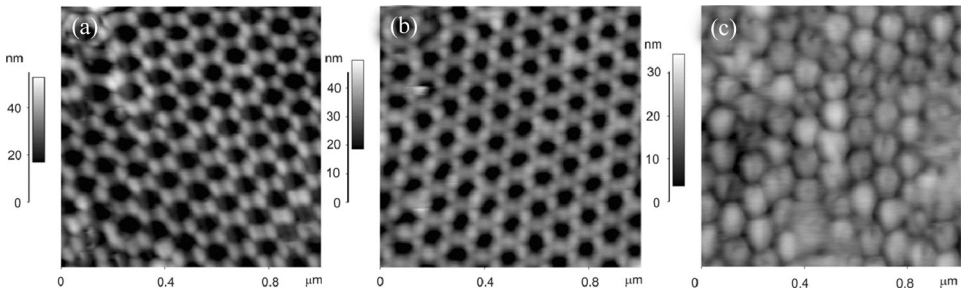

Figure 4. AFM micrographs of oxalic AAM: (a) the porous cap, (b) the opened barrier layer (completing the nanotube arrays), and (c) bent-core filled AAM-nanotubes giving rise to the hybrid 1D ordered nanocomposite.

PFB-cromophores inside the nanometric pores according to the implemented mechanically induced insertion-method. On the other hand, a more detailed inspection of the micrograph displayed in Figure 4(c) (from digitalized amplified images), shows that the guest molecules tend first to aggregate on the walls of the nanotubes in order to find mechanical support after drying; for this reason some nanopores seem to be partially filled with a small hole in the middle. Chemical interactions between the **PFB**-molecules and the AAM-nanotubes are also possible as it is discussed in next section. Indeed, the bent-core molecule was not easily removed from the AAM by washing the hybrid sample with different solvents (THF and toluene), even after dipping the hybrid for several days in these solvents, an important part of these **PFB**-molecules remained inside the AAM. This fact demonstrates a strong mechanical interaction between this compound and the AAM. These observations strongly suggest chemical interactions of these **PFB**-compounds with the AAM, including possible atomic binding as it is discussed in next section.

3.2. *Spectroscopic Measurements*

In addition to the AFM/morphological characterization, comparative spectroscopic studies such as UV-Vis linear absorption, PL- and Raman-spectroscopies were implemented in order to verify the insertion of the **PFB**-molecules inside the AAM-nanotubes and the optical performance of the hybrids. In fact, the AAM:PFB hybrids were obtained from saturated Toluene-dissolutions in order to achieve highest possible molecular loading inside the AAMs; hence details of the absorption bands of the implemented **PFB**-molecules within the AAM environment can be easily recognized when comparing the spectral features of the **PFB** doped AAMs with the reference AAM-sample and with an unsaturated PFB/Toluene dissolution.[1] **PFB** shows an intense yellow color in the powder state and produces a cloudy opaque AAM hybrid which is evident from the comparative linear absorption spectra shown in Figure 5.

It is observed that the PR-AAM is fully transparent within the Vis-NIR region, showing only moderate absorption to the UV region. This fact reveals suitable

[1]A slightly PFB loaded, partially transparent toluene solution was prepared in order to assure that the Beer–Lambert law applies in UV-Vis spectral measurements.

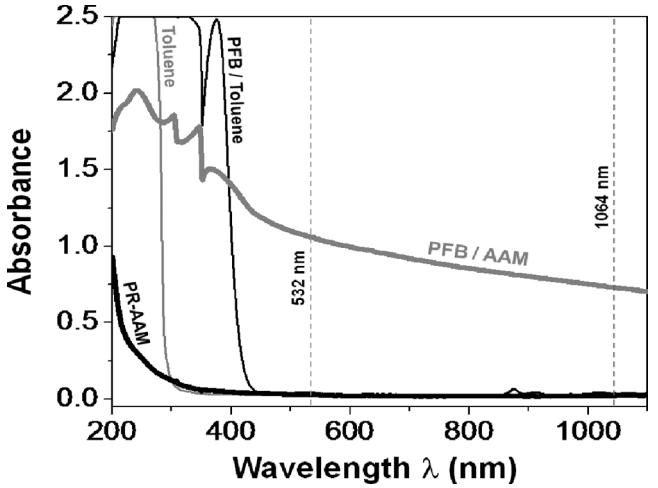

Figure 5. Comparative absorption spectra at room temperature of: a pure reference AAM sample (PR-AAM), a PFB/Toluene dissolution, the Toluene solvent and a PFB doped AAM sample (PFB/AAM).

conditions for using these AAM-templates in several optical applications. This wide high-transmission window also demonstrates the high optical and chemical purity achieved by the AAM network via the oxalic route. Thus, it can be assured that the absorption bands observed for the hybrids are mainly due to the organic part of the composite and that the AAM-matrix does not contribute to the absorption spectrum of the hybrid structure. In fact, typical features of the **PFB** in solution can be observed in the solid state doped AAM. In general, the **PFB** based hybrid exhibit absorption bands within the 280–428 nm spectral range and shows a drastically enhanced and monotonically decreasing tail from 433 to 1100 nm. If we compare the absorption bands of the **PFB** compound in solution and in the AAM-network, a notable blue shift from the solution spectra to the solid hybrid phase can be observed. For instance, the main peak observed in solution at $\lambda_{max} = 376$ nm, appears at $\lambda_{max} = 364$ nm in the respective **PFB**-based hybrid (12 nm blue shifted). This blue shift is an indication of a lowered charge transfer character of the **PFB** compound within this environment; however, since the **PFB** doping concentration increases in the solid state, this favors the aggregation/reorganization phenomena of the bent-core molecules inside the nanotubes. The appearance of the long tail in the AAM-phase may also be indicative of possible interactions between the AAM network and the bent-core compound which break the symmetry, this effect should be further investigated in future investigations via special techniques such as XPS (X-ray photo-electron spectroscopy). The hybrid samples were also studied under strong IR-laser irradiation in order to estimate their quadratic NLO-SHG properties. In this context, the available laser excitation line (at $\lambda_\omega = 1064$ nm) and the NLO-line at the SHG wavelength ($\lambda_{2\omega} = 532$ nm) are also shown in Figure 5.

PL-spectra show higher emission activity for the PFB/AAM hybrid sample, although no special features of the bent-core compound can be identified in the solid state (see Figure 6). In fact, the **PFB** compound in toluene and the PR-AAM

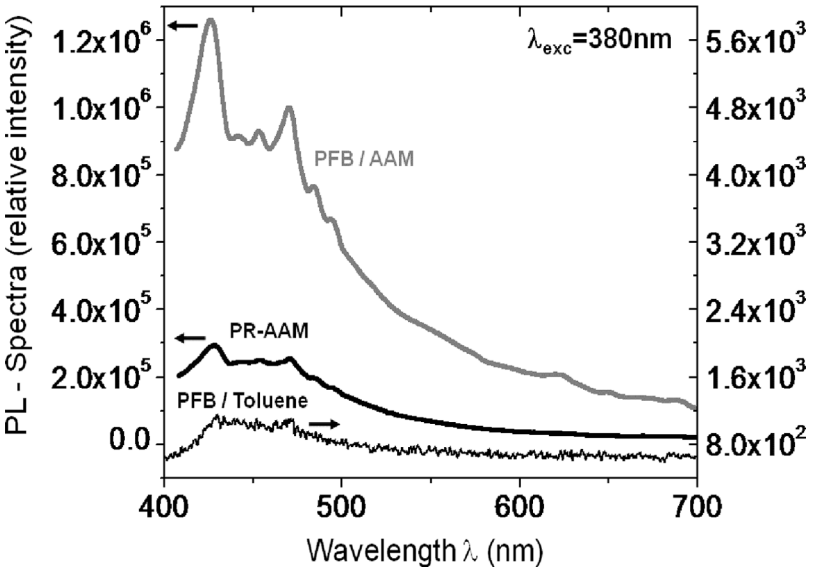

Figure 6. Comparative PL-spectra (not normalized) at room temperature obtained for: a pure reference AAM sample (PR-AAM), a PFB/Toluene solution, and a PFB doped AAM sample (PFB/AAM).

network inopportunely show similar spectral features with significantly weaker PL-activity of the former one. The main difference arises from the considerable stronger PL-emission of the **PFB** doped AAM, which exhibit enhanced features of both materials. Indeed, in the solid-state molecular concentration is higher which may substantially increase the emission of the doped AAM-sample, indicative of adequate guest molecular loading.

In Figure 7, the Raman-fluorescence signals obtained from the reference PR-AAM, the **PFB** doped AAM sample (PFB/AAM) and a **PFB**-powder sample are displayed. Emissions of the PR-AAM exhibit an increasing linear, monotonic dependence with the wave number, without any significant variation and defined sharp peaks. By contrast, Raman emissions measured from the pristine, non-confined compound (powder sample) show a complex fluorescence/Raman spectrum, composed by several bands characteristic of the **PFB** molecular compound. It is noted that the strongest fluorescence emission appears for this sample, dominating the emission spectra of both the hybrid composite and reference PR-AAM. Finally, the Raman spectra of the hybrid structure (PFB/AAM) exhibit considerable lower intensity emissions than those observed for the pristine and PR-AAM samples. However, the main features of the hybrid composite correspond very well to the emission peaks of the pristine, non-confined molecules (see Raman peaks within the grey bars for comparison). This fact, unambiguously demonstrates the abundant presence of the guest molecular structures inside the membrane nanotubes and on its respective layer (as shown by AFM-measurements). As mentioned before, due to the highly absorptive characteristics of the studied **PFB**-compound (see Fig. 5), the stronger Raman emission of the PR-AAM is drastically absorbed by the guest **PFB**-molecules contained in the hybrid samples which produces weaker Raman signals for the PFB-based hybrid.

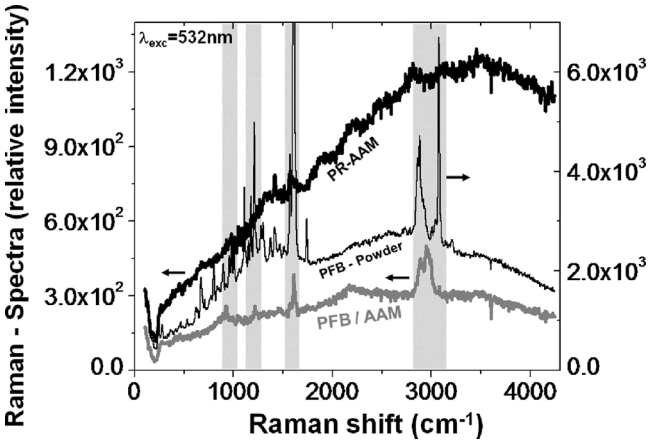

Figure 7. Comparative Raman-spectra (not normalized) at room temperature obtained for: a pure reference AAM sample (PR-AAM), a pristine PFB-powder sample, and a PFB doped AAM sample (PFB/AAM).

3.3. *NLO – Measurements*

Finally, a NLO-SHG test was performed to the PFB/AAM-hybrid system in order to investigate the quadratic NLO performance of such geometric nano-arrays, and most importantly, the possible molecular ordering of the LC-compounds inside the AAM at room temperature. In fact, measurable SHG signals were detected for the hybrid samples, indicating an anomalous and stimulated ordering of the guest molecules induced by the nanotube walls during insertion and sample drying. Figure 8(a) shows typical SHG-measurements directly taken from the oscilloscope

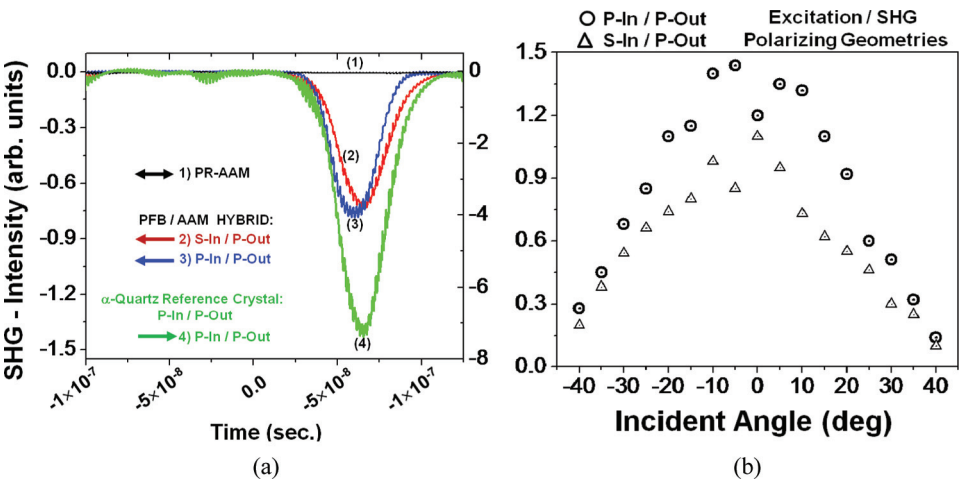

(a) (b)

Figure 8. Comparative SHG-signals measured from a PFB doped AAM sample (PFB/AAM): (a) Oscilloscope screen shot displaying the SHG-activity of a pure reference AAM sample (PR-AAM), the hybrid structure under different polarizing geometries and the quartz reference crystal, and (b) Angle dependent SHG-measurements performed in the PFB/AAM hybrid samples at parallel and orthogonal polarizing geometries.

screen (at normal laser incidence) performed in both P-In/P-Out and S-In/P-Out laser beam polarization geometries. Since it is generally accepted that the walls of the nanotubes are conformed by an amorphous centro-symmetric structure, formed by the aggregation of nanoparticles with sizes ranging from 2.5 to 4 nm and conformed by tetra and hexacoordinated aluminum (AlO_4 and AlO_6 polyhedral units) [51,52], no SHG is produced by the PR-AAM. Only very weak and negligible surface SHG-effects (generally detected by Lock-In amplification) may arise due to the symmetry breakdown typical of surfaces and interfaces or according to the quadrupole-moment mechanism [53,54]. This amorphous structure has been verified in our reference samples by X-ray diffraction (XRD) measurements (not shown here, [49]) where a broad XRD-spectra has been observed. By contrast, strong and quite similar SHG-signals can be obtained from the hybrid structures in both P-In/P-Out and S-In/P-Out polarizing geometries. Indeed, it has been documented that bent-core room temperature phases like the B_4-phase (or Sm-B phase) exhibit strong SHG [37,38,40,55]. Nevertheless, several and contradicting proposals have been given for the explanation of this phenomenon which still makes this phase object of debate. In this respect, some authors, on the basis of some similarities between this phase and the twisted-grain-boundary (TGB) ones, suggested the existence of helical arrangements with the helix axis parallel to the smectic layers [34,35,39]. Additional studies performed by AFM surface imaging reveals smectic layers in ''worm-like'' structures that tend to form a superimposed periodical orientation order and helical superstructures [56]. Alternatively, other authors disagreed with the previous works and explained the structure and the SHG activity in terms of some birefringent inclusions that could be metastable glassy states of polar nature created at the $B_2 - B_4$ transition [55]. In this case, an optically isotropic phase that presents two types of domains with opposite chirality and a very high optical activity is proposed. Moreover, it is stated that the phase does not present SHG intrinsically, being the detected signal caused by the remanent polar glassy states. Finally, in a work carried out by Kentischer *et al.* [57], the authors proposed a non-centrosymmetric glassy state for this phase. They observed SHG in this phase and estimated a d_{eff} value as high as 1 pm V^{-1}. To explain this result, a structure made up of randomly oriented domains, with spontaneous polar order, was suggested. A remarkable property of the room temperature B_4 – phase is the fact that the emergence of SHG activity does not require application of any external electric fields. Therefore a glassy or crystalline polar structure can be proposed for these domains, where the whole SHG signal must be obtained by incoherently summing the SHG intensities produced by all the randomly oriented inclusions. In an attempt to summarize and conciliate the different interpretations, it can be stated that this phase exhibit a smectic mesogenic behavior formed by a nontilted in-plane order, but this phase is not a crystal; thus the existence of a spontaneous non-centrosymmetric polar order give rise to measurable SHG [38].

From our measurements, a SHG-intensity dependence with the incidence angle (see Fig. 8(b)) can be observed; here highest SHG conversion occurs at nearly normal incidence with slightly larger SHG-signals detected for the P-In/P-Out polarizing geometry (although these small differences may be irrelevant considering the estimated experimental error of ~15%). On the other hand, it has been noted that the SHG-signals did not depend on the polarization direction of the incident fundamental beam. This result was confirmed in different areas of the sample and also in several specimens. In order to further verify the SHG dependence with the

polarizer-analyzer polarizing geometries, SHG polar measurements were performed by varying the polarizer angle, as it is shown in Figure 9. Again, only small differences in the SHG-signals from the P-In/P-Out (parallel) and P-In/S-Out (orthogonal) polarizing geometries can be detected, resulting in a nearly circular polar SHG-plot. These results may suggest the formation of multipolar and cylindrical superimposed smectic layers (jelly-roll configuration), similar to those proposed for higher temperature switchable phases of bent-core fibers [58]. In our case, the analogous but narrower cylindrical nanotube confinement may force the bent core compounds to adopt comparable geometries. Under such strong multipolar molecular nano-packing, a minor dependence of the different implemented polarizing geometries and excitation configurations should be observed for the SHG output intensities. The decrease of the SHG-signals with increasing incident angles may also be partially explained considering a minor contribution of the multipoles at such excitation conditions; this may be attributed to a less effective cross-section excitation of the jelly-roll configuration, to a minor material interaction length and to interference effects with several parallelely aligned, non-active AAM-nanotube walls. In such wide-angle excitation conditions, the incoherently sum of the SHG-intensities produced by all the **PFB**-loaded nanotubes within the interaction length must be diminished.

Finally, in order to give an estimate of the SHG conversion efficiency generated by the hybrid structure, a relative SHG-signal calibration was performed taking into account the SHG-signal (phase-matched configuration) provided by the reference α-quartz crystal at same experimental conditions (see Fig. 8(a)). Due to the stronger absorption of the hybrid samples at the SHG-wavelength, compared to the transparent mono-crystalline quartz reference, self-absorption effects of the hybrid samples limit its SHG-efficiency. In fact, in case of the hybrid PFB/AAM structure a NLO-SHG conversion efficiency of about 10% of the reference sample is detected.

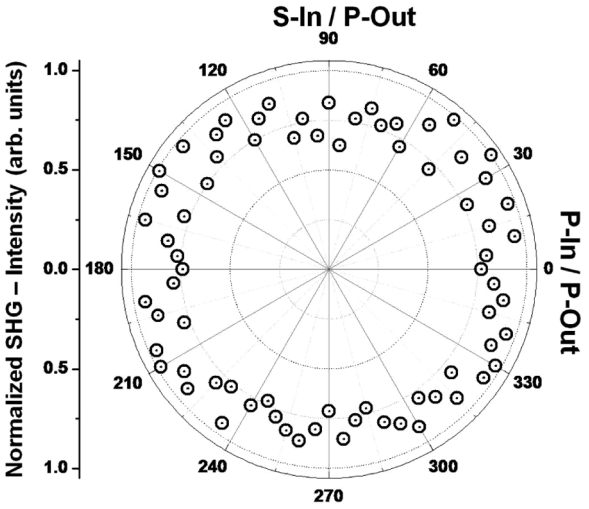

Figure 9. Polarizing dependent SHG measurements performed in a PFB doped AAM sample (PFB/AAM): the polarizer axis is rotated toward the analyzer axis (fixed at P-position) from a starting parallel (P-In/P-Out, 0°) configuration to a perpendicular one (S-In/P-Out, 90°), completing the polar plot up to 360°.

This frequency doubling achieved by the hybrid sample represents in any case a notable SHG-conversion efficiency. On the other hand, the angle dependent SHG measurements (see Fig. 8(b)) does not exhibit any significant oscillating behavior (usual for non-phase matched Maker-Fringes experiments); this is partially due to the relatively strong absorptive media at the SHG wavelength. For these reasons only the average effective $\chi^{(2)}_{eff}$ parameter was evaluated by direct comparison to the reference quartz sample and according to Eq. (1):

$$\chi^{(2)-Hybrid}_{eff} \propto \chi^{(2)-Quartz}_{11}\left(\frac{2l_c^{Quartz}}{\pi l^{Membrane}}\right)\left[\frac{I^{Hybrid}_{2\omega}}{I^{\chi^{(2)}_{11}-Quartz}_{2\omega}}\right]^{1/2}, \quad (1)$$

where l_c^{Quartz} is the coherence length of the quartz crystal ($\approx 22\,\mu m$), $l^{Membrane}$ is the AAM membrane thickness and $I^{\chi^{(2)}_{11}-Quartz}_{2\omega}$ is the SHG-intensity at maximum of the *Maker*-Fringes observed for the reference crystal (at optimal phase matching conditions). The estimated NLO $\chi^{(2)}_{eff}$ -macroscopic susceptibility coefficient evaluated according to this approximation (derived from the Maker-Fringes method) for the hybrid sample is in the order of $\chi^{(2)}_{eff} \approx 0.4\,pm/V$ (an estimated experimental error of about 15% is considered). This result agrees well with previously reported data. Nevertheless, additional investigations should be performed in order to further understand the role played by the AAM-nanotubes in the fabrication of the studied hybrid systems for optical applications, as well as the molecular interactions between guest and host systems and the orientational order and symmetry properties achieved by the bent-core compounds within this kind of confinement. Additionally, thermo-optical and EO-studies in the different mesophases of the PFB/AAM based hybrids and the molecular thermal insertion process should also be investigated in order to further understand the physical characteristics of the PFB-molecules within the AAM nanotube-like confinement. Such experiments are currently underway and will be published in the near future as a continuation of this contribution.

4. Conclusions

In this work, the powder structure of the **PFB**-molecules (exhibiting B_4–phase) was used as received in Toluene-dissolutions in order to fabricate the AAM/PFB-nanotube based hybrid systems at room conditions. According to our results, it has been shown that the mechanically induced insertion of PFB-LC into the nanotube arrays of prepared oxalic AAM was successfully achieved as monitored by AFM-imaging, absorption and Raman/fluorescence spectroscopies, and by the NLO-SHG technique. According to these techniques, extreme molecular inclusion is confirmed within the host AAM-nanotubes implementing the fluorinated bent-core compounds in convenient Toluene:dopant dissolutions. Despite the absorption effects displayed by the PFB/AAM based hybrids at the SHG wavelength, non negligible SHG signals were measured on these hybrid samples exhibiting highest quadratic NLO coefficient in the order of $\chi^{(2)}_{eff} \approx 0.4\,pm/V$ which was estimated according to a simplified straightforward calibration method. The analysis of the SHG signals performed under several experimental conditions showed that the quadratic NLO-response obtained from such complex hybrid systems did not depend on the excitation polarizing geometry or relative polarizer-analyzer

configuration. We argue that the obtained results point out to a complex but interesting molecular ordering of a multipolar nature which should be further investigated. Indeed, since this research reports the starting point to the study of the mesogenic and optical behavior of bent core compounds confined in AAM-nanotubes, there are still a number of unsolved questions which have to be systematically solved in future and complementary investigations. Finally, we believe in accordance to other authors, that the ordered AAM hybrid structures represent a promising field of investigation in the route to functional bent core LC-based materials [59,60].

Acknowledgments

One of the authors (O. G. Morales-Saavedra) acknowledges financial support from the DAAD academic organization (Germany) and to the PAPIIT-DGAPA-UNAM (grant IN-IN115508).

References

[1] Boyd, R. W. (2002). *Nonlinear Optics*, Academic Press: San Diego, CA, USA.
[2] Saleh, B. E. A. *et al.* (2006). *Fundamentals of Photonics*, John Wiley and Sons Ltd.: New York, USA.
[3] Prasad, P. N. *et al.* (1991). *NLO Effects in Molecules and Polymers*, John Wiley and Sons Ltd: New York, USA.
[4] Nalwa, H. S. *et al.* (1997). *Non-linear Optics of Organic Molecules*, CRS Press Inc.: Boca Raton, Florida, USA.
[5] Zyss, J. (1994). *Molecular Nonlinear Optics: Materials, Physics and Devices*, Elsevier Science & Technology: Boston, USA.
[6] Kajzar, F. *et al.* (1996). *Organic Thin Films for Waveguiding Non-linear Optics*, Gordon and Breach Publishers: San Jose, CA, USA.
[7] Morales-Saavedra, O. G., Mata-Zamora, M. E., Rivera, E., Bañuelos, J. G., & Saniger, J. M. (2008). *J. Dyes and Pigments*, *78*, 48.
[8] Morales-Saavedra, O. G., Rivera, E., Flores-Flores, J. O., Castañeda, R., Bañuelos, J. G., & Saniger, J. M. (2007). *J. Sol-Gel Sci. Technol.*, *41*(3), 277.
[9] Diggle, J., Downie, W., & Goulding, C.W. (1969). *Chem. Rev.*, *69*, 365.
[10] Thompson, G. E., Furneaux, R. C., Wood, G. C., Richardson, J. A., & Goode, J. S. (1978). *Nature*, *272*, 433.
[11] Martin, C. R. (1994). *Science*, *266*, 1961.
[12] Rutkevitch, D., Tager, A. A., Haruyama, J., Almawlawi, D., Moskovits, M., & Xu, J. M. (1996). *IEEET. Electron Devices*, *43*(10), 1646.
[13] Li, A. P., Müller, F., Birner, A., Nielsch, K., & Gösele, U. (1998). *J. Appl. Phys.*, *84*(11), 6023.
[14] Nielsch, K., Choi, J., Schwirn, K., Wehrspohn, R. B., & Gösele, U. (2000). *Nano Letters*, *2*(7), 677.
[15] Lajos, G. (1997). *Characterization and Optical Theory of Nanometal/porous Alumina Composite Membranes*. Ph.D. Thesis, The University of Colorado, Colorado, U.S.
[16] Xu, T. T., Piner, R. D., & Ruoff, R. S. (2003). *Langmuir*, *19*, 1443.
[17] Sui, Y. C., González, J. A., Bermúdez, A., Acosta, D., Feuchtwanger, R. J., Flores, J. O., Cui, B. Z., Mata, M. E., & Saniger, J. M. (2001). *Mat. Res. Soc. Symp.*, *633*(A13.51.1–A13.51.8).
[18] Zhang, X. Y., Zhang, L. D., Li, G. H., & Zhao, L. X. (2001). *Mat. Sci. Eng. A.*, *308*, 9.
[19] Iwasaki, T., Motoi, T., & Den, T. (1999). *Appl. Phys. Lett.*, *75*(14), 2044.

[20] Paulus, P. M., Luis, E., Kröll, M., Schmid, G., & Jongh, L. J. J. (2001). *Magn. Magn. Mater.*, *224*, 180.
[21] Lei, Y., Liang, C. H., Wu, Y. C., Zhang, L. D., & Mao, Y. Q. (2001). *J. Vac. Sci. Technol. B.*, *19*(4), 1109.
[22] Shi, G., Mo, C. M., Cai, W. L., & Zhang, L. D. (2000). *Solid. State. Comm.*, *115*, 253.
[23] Zhou, Y., Shen, C., & Li, H. (2002). *Solid State Ionics*, *146*, 81.
[24] Klein, J. D., Herrick, R. D., Palmer, D., Sailor, M. J., Brumlik, C. J., & Martin, C. R. (1993). *Chem. Mater.*, *5*, 902.
[25] Fukuda, Y., & Fukushima, T. (1980). *Bull. Chem. Soc. Jpn.*, *53*, 3125.
[26] Ozao, R., Ochiai, M., Ichimura, N., Takahashy, H., & Inada, T. (2000). *Thermochim. Acta*, *352/353*, 91.
[27] Mardilovich, P. P., Govyadinov, A. N., Mukhurov, N. I., Rzhevskii, A. M., & Paterson, R. (1995). *J. Membrane Sci.*, *98*, 131.
[28] Thompson, G. E., & Wood, G. C. (1981). *Nature*, *290*, 230.
[29] Yamamoto, Y., & Baba, N. (1983). *Thin Solid Films*, *101*, 329.
[30] Vorländer, D. (1929). *Ber. Dt. Chem. Ges.*, *65*, 2831.
[31] Vorländer, D., & Apel, A. (1932). *Ber. Dt. Chem. Ges.*, *62*, 1101.
[32] Matsuzaki, Y., & Matsunaga, I. (1993). *Liq. Cryst.*, *14*, 105.
[33] Akutagawa, T., Matsunaga, Y., & Yasuhara, K. (1994). *Liq. Cryst.*, *17*, 659.
[34] Niori, T., Sekine, T., Watanabe, J., Furukawa, T., & Takezoe, H. (1996). *J. Mater. Chem.*, *6*, 1231.
[35] Sekine, T., Niori, T., Sone, M., Watanabe, J., Choi, S. W., Takanishi, Y., & Takezoe, H. (1997). *Jpn. J. Appl. Phys.*, *36*, 6455.
[36] Link, D. R., Natale, G., Shao, R., Maclennan, J. E., Clark, N. A., Körblova, E., & Walba, D. M. (1997). *Science*, *278*, 1924.
[37] Pelzl, G., Diele, S., & Weissflog, W. (1999). *Adv. Mater.*, *09*, 707.
[38] Takezoe, H., & Takanishi, Y. (2006). *Jpn. J. Appl. Phys.*, *45*(2A), 597.
[39] Watanabe, J., Niori, T., Sekine, T., & Takezoe, H. (1998). *Jpn. J. Appl. Phys.*, *37*, L139.
[40] Rauch, S., Selbmann, Ch., Bault, P., Sawade, H., Heppke, G., Morales-Saavedra, O., Huang, M. Y. M., & Jákli, A. (2004). *Phys. Rev. E.*, *69*, 021707.
[41] Morales-Saavedra, O. G., Jákli, A., Heppke, G., & Eichler, H. J. (2006). *J. Nonl. Opt. Phys. Mat.*, *15*(4), 431.
[42] Jákli, A., Prasad, V., Shankar Rao, D. S., Liao, G., & Jánossy, I. (2005). *Phys. Rev. E.*, *71*, 021709.
[43] Morales-Saavedra, O. G., Bulat, M., Rauch, S., & Heppke, G. (2004). *Mol. Cryst. Liq. Cryst.*, *413*, 607.
[44] Eremin, A., Diele, S., Pelzl, G., Nadasi, H., & Weissflog, W. (2003). *Phys. Rev. E*, *67*, 021702.
[45] Schröder, M. W., Pelz, G., Donemann, U., & Weissflog, W. (2004). *Liq. Cryst.*, *31*, 633.
[46] Kinoshita, Y., Park, B., Takezoe, H., Niori, T., & Watanabe, J. (1998). *Langmuir*, *14*, 6256.
[47] Nalwa, H. S., Watanabe, T., & Miyata, S. (1995). *Adv. Mater.*, *7*, 754.
[48] Morales-Saavedra, O. G., Jákli, A., Heppke, G., & Eichler, H. J. (2006). *J. Nonl. Opt. Phys. Mat.*, *15/2*, 287.
[49] Mata-Zamora, M. E., & Saniger, J. M. (2005). *Rev. Mex. Fis.*, *51*(5), 502.
[50] Li, A. P., Müller, F., Birner, A., Nielsch, K., & Gösele, U. (1999). *J. Vac. Sci. Technol.*, *A17*(4), 1428.
[51] Partermarakis, G., Moussoutzanis, K. (1999). *J. Appl. Catal. A General*, *180*, 345.
[52] Farnan, I., Dupree, R., Jeong, Y., Thompson, G. E., Wood, G. C., & Forty, A. J. (1989). *Thin Solid Films*, *173*, 209.
[53] Zhong-Can, O. Y., & Yu-Zhang, X. (1985). *Phys. Rev. A*, *32*, 1189.
[54] Shtykov, N. M., Barnik, M. I., Beresnev, L. A., & Blinov, L. M. (1985). *Mol. Cryst. Liq. Cryst.*, *124*, 379.

[55] Ortega, J., Pereda, N., Folcia, C. L., Etxebarria, J., & Ros, M. B. (2000). *Physical Review E*, *63*, 011702.
[56] Heppke, G., & Moro, D. (1998). *Science*, *279*, 1872.
[57] Kentischer, F., Macdonald, R., Warnick, P., & Heppke, G. (1998). *Liq. Cryst.*, *25*, 341.
[58] Jákli, A., Krüerke, D., & Nair, G. G. (2003). *Physical Review E*, *67*, 051702.
[59] Etxebarria, J., & Ros, M. B. (2008). *J. Mater. Chem.*, *18*, 2919.
[60] Ros, M. B., Serrano, J. L., de la Fuente, M. R., & Folcia, C. L. (2005). *J. Mater. Chem.*, *15*, 5093.